ELSEVIER

Catalysis Today 61 (2000) 73–85

CATALYSIS TODAY

www.elsevier.com/locate/cattod

A two-phase compartments model for the selective oxidation of *n*-butane in a circulating fluidized bed reactor

Shantanu Roy [a,*], M.P. Duduković [a,1], Patrick L. Mills [b,2]

[a] *Department of Chemical Engineering, Chemical Reaction Engineering Laboratory, Washington University, St. Louis, MO 63130-4899, USA*
[b] *DuPont Company, Experimental Station, E304/A204, Central Research and Development, Wilmington, DE 19880-0304, USA*

Abstract

A phenomenological model for the partial oxidation of *n*-butane to maleic anhydride (MAN) in a gas–solid riser reactor is proposed. The model captures the main transport–kinetic interactions at both the particle and reactor scale. Two different kinetic models from the literature that either include or neglect the role of solid-state diffusion of oxygen in the catalyst bulk are compared in terms of their impact on overall reactor performance. The use of computational fluid dynamics (CFD) as a means of defining a macroscopic cell-type model for describing the flow patterns in an industrial-scale gas–solids riser is also described. Predictions for the conversion of *n*-butane and yield of MAN are presented as a function of selected operating variables, and the impact of the variable model parameters on the predictions is briefly assessed. It is shown that the predictions are particularly sensitive to the kinetic model. The relative importance of the interactions between the chemical kinetics and the hydrodynamics is also highlighted. © 2000 Published by Elsevier Science B.V.

Keywords: Selective oxidation; *n*-Butane; Bed reactor; Maleic anhydride

1. Introduction

Maleic anhydride (MAN) ($C_4H_2O_3$) was first commercially manufactured in the early 1930s by the vapor phase oxidation of benzene (C_6H_6) [1]. Most processes now use *n*-butane as the hydrocarbon source with vanadium phosphorus oxide (VPO) catalysts. In the past three decades, various reactor configurations, such as packed beds [2], fluidized beds [3] and risers [4–6] have been commercialized. These various reactor types have different gas–solid flow patterns that interact with the complex chemistry of *n*-butane oxidation over VPO catalysts to ultimately give different yields of MAN. The DuPont *n*-butane-to-THF process uses a riser reactor with physically separated catalyst oxidation and reduction zones, rapid recovery of catalyst, and more uniform temperature, so that better reactor performance is claimed. The impact of gas and solids phase backmixing, catalyst attrition, heterogeneity in the solids distribution, interparticle and intraparticle transport effects, finite transport rates of lattice oxygen in the catalyst bulk, and gas phase homogeneous combustion reactions on the reactor performance has not been widely studied, however. The objective of this work is to assess the effect of some of these factors in determining the overall reactor performance as part of a larger effort to quantify the interactions between kinetics, transport effects and hydrodynamics.

* Corresponding author. Tel.: +1-314-935-6042.
E-mail addresses: shunt@wuche.che.wustl.edu (S. Roy), dudu@wuche2.che.wustl.edu (M.P. Duduković), patrick.l.mills@usa.dupont.com (P.L. Mills).
[1] Tel.: +1-314-935-6021; fax: +1-314-935-4832.
[2] Tel.: +1-302-695-8100; fax: +1-302-695-3501.

0920-5861/00/$ – see front matter © 2000 Published by Elsevier Science B.V.
PII: S0920-5861(00)00352-7

Nomenclature

c_{B_0}	initial *n*-butane concentration in gas phase (mol m^{-3})
c_{tot}	concentration of active lattice oxygen sites in the VPO catalyst (mol/kg-cat.)
C	concentration of species (mol m^{-3})
D	diameter of catalyst particle (m)
e	restitution coefficient (dimensionless)
g_0	radial distribution function (dimensionless)
k_{Θ_s}	granular thermal conductivity (kg m^{-1} s^{-1})
K	volumetric exchange coefficient (in reactor model) (m^3 s^{-1})
K	momentum exchange coefficient (in CFD model) (kg m^{-3} s^{-1})
p	pressure (N m^{-2})
Q_s	solids flow rate (kg s^{-1})
r_{red}	rate of reduction on catalyst surface (depletion rate of lattice oxygen sites) (mol/(kg-cat.)-s)
Re	Reynolds number (dimensionless)
$\bar{R}_{h,i}$	rate of depletion of species i by heterogeneous reaction (mol m^{-3} s^{-1})
$\bar{R}_{s,i}$	rate of depletion of species i by heterogeneous reaction (mol/(kg-cat.)-s)
t	time (s)
u	velocity (m s^{-1})
V_g	volume of each gas compartment (m^3)
W_s	solids inventory in each solids compartment (kg)

Greek symbols

α	volume fraction or holdup
γ	collisional energy dissipation rate (kg m s^{-3})
θ	lattice oxygen concentration (dimensionless)
Θ	granular pseudo-thermal temperature (m^2 s^{-2})
μ	viscosity (kg m^{-1} s^{-1})
ξ	radial coordinate in catalyst particle (dimensionless)
ρ	density (kg m^{-3})
ρ_b	bulk density of catalyst (kg m^{-3})
τ	shear stress (N m^{-2})
ϕ	collisional energy dissipation rate due to fluid–solid interactions (kg m^{-1} s^{-3})

Subscripts/superscripts

f	continuous fluid phase
g	gas phase
i	species index
j, q	index for the solids compartment
k, p	index for the gas phase compartment (in reactor model)
k	index for phase (in CFD model)
s	(dispersed) solid phase

1.1. Reaction kinetics

The riser model set forth in the next section requires a model for the kinetics of *n*-butane to MAN. The particular kinetic models used here are described below.

The reaction kinetics of *n*-butane over VPO has been the subject of numerous investigations [2,7–21]. It is generally agreed that the global heterogeneous reaction kinetics can be described by the following triangular network of reactions where the desired reaction involves transfer of 14 electrons to produce MAN via Eq. (1):

$$n\text{-}C_4H_{10} + 3.5O_2 \rightarrow \text{MAN} + 4H_2O \quad (1)$$

$$\text{MAN} + 4.5O_2 \rightarrow 4CO_2 + H_2O \quad (2)$$

$$n\text{-}C_4H_{10} + 4.5O_2 \rightarrow 4CO + 5H_2O \quad (3)$$

The above-cited body of literature suggests that considerable research activity in the last decade has been focussed on unraveling the kinetic mechanism for this reaction system. Of particular interest here is the widely cited work of Centi et al. [11] in which the reaction mechanism was extracted from isothermal steady-state tubular fixed bed reactor data in which the oxygen was supplied to the catalyst from the gas phase (Table 1).

Subsequent investigations by Bej and Rao [15–18] led to the development of a redox partial oxidation reaction model that was zero order in oxygen partial pressure and first order in *n*-butane partial pressure. Recently, Mills et al. [21] investigated the redox kinetics of both γ-$VOPO_4$ and δ-$VOPO_4$ pure phases using the TAP (Temporal Analysis of Products®) system

Table 1
Kinetic parameters from Centi et al. [11][a]

Temperature	380°C (653 K)
n-$C_4H_{10} \rightarrow$ MAN	$r_1 = r_{MAN} = \frac{k_1 K_B c_B {c_0}^{\alpha}}{1 + K_B c_B}$
n-$C_4H_{10} \rightarrow CO_2$	$r_2 = r_{CO_2} = k_2 {c_0}^{\beta}$
MAN $\rightarrow CO_2$	$r_3 = -r_{MAN} = k_3 c_{MAN} \left(\frac{{c_o}^{\gamma}}{{c_B}^{\delta}}\right)$
k_1	2.191×10^{-4} mol$^{1-\alpha}$ (m^3)$^{\alpha}$/(kg-cat.)-s
K_2	7.028×10^{-5} mol$^{1-\beta}$ (m^3)$^{\beta}$/(kg-cat.)-s
K_3	4.989×10^{-6} mol$^{\delta-\gamma}$ (m^3)$^{1+\gamma-\delta}$/(kg-cat.)-s
K_B	2.616 m^3/mol
α	0.2298
β	0.2298
γ	0.6345
δ	1.151

[a] Note that units (SI) are different from original paper (CGS).

[22]. It was shown that the reduction of these particular fully re-oxidized pure $VOPO_4$ catalyst phases using *n*-butane can be described by a reaction rate form that is first order in *n*-butane and approximately one-third order in the concentration of surface lattice oxygen. During a reduction cycle, the lattice oxygen species on the catalyst surface react with *n*-butane, which establishes a positive gradient for solid-state diffusion of sub-surface lattice oxygen from the catalyst bulk to the surface. During the catalyst regeneration process with air, the vacancies created by reduction are supposed to be filled with oxygen. The impact of solid-state diffusion on reactor performance is suspected but not well documented. The primary objective here is to assess the impact of this mechanism on the overall reactor performance, and to compare the results with those based on the kinetics of Centi et al. [11].

1.2. Riser hydrodynamics

The flow patterns of the gas and solids in a riser are generally complex [23]. A complete riser reactor model would involve the simultaneous solution of the two-phase Navier–Stokes equations including turbulence, drag and solid phase collisional models, and a detailed particle-scale model for the reaction kinetics. Even if the reaction kinetics were available, the resulting stiff sets of equations would be computationally intractable at the present time.

In this work, an alternative approach for modeling the partial oxidation of *n*-butane in a riser reactor is used in which the fundamental models of the hydrodynamics and the chemistry are decoupled. By solving for the macroscopic field variables using computational fluid dynamics (CFD) techniques, the overall gas and solid flow patterns are extracted and used to assess the impact of coupling with detailed kinetic models on overall reactor performance.

2. Model development

The model developed here is a phenomenological one and does not explicitly account for the local spatial distribution of the solids in the riser. It is based upon a series of mixing cells in which the extent of backmixing is described using *M* cells for the solid phase and *N* cells for the gas phase where the total number of cells for each phase is treated as a variable parameter. Additional aspects on the model development are given below.

2.1. Assumptions

The detailed assumptions made in the development of the model are as summarized below. A schematic diagram of the model is given in Fig. 1.

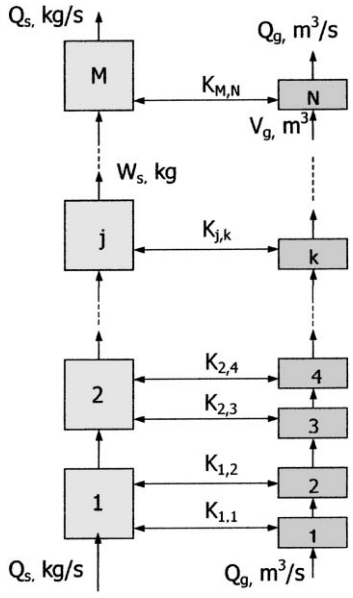

Fig. 1. Schematic diagram of the model formulation.

Table 2
Kinetic parameters calculated from Mills et al. [21]

Temperature		380°C (653 K)
n-$C_4H_{10} \rightarrow$ MAN	(1)	
n-$C_4H_{10} \rightarrow CO_2$	(2)	$r_i = k_i c_B \theta_{0,s}^{\gamma_i}$
n-$C_4H_{10} \rightarrow$ CO	(3)	
k_1		1.43×10^{-4} mol$^{-\gamma_1}$ m^3/(kg-cat.)$^{1-\gamma_1}$-s
K_2		1.23×10^{-4} mol$^{-\gamma_2}$ m^3/(kg-cat.)$^{1-\gamma_2}$-s
K_3		7.47×10^{-4} mol$^{-\gamma_3}$ m^3/(kg-cat.)$^{1-\gamma_3}$-s
γ_1		0.41
γ_2		0.87
γ_3		1
V–V lattice distance		4.5 Å
Concentration of active V sites		10.4 mol/kg-cat.

- Both the solids (M cells) and the gas phase (N cells) are modeled as a series of mixing cells with exchange where the total number of tanks can be adjusted to define the state of backmixing in each phase. In general, the gas is assumed to be less backmixed than the solids, which is based upon experimental studies of gas and solid phase mixing in risers [24].
- The interphase transfer of reactant and product species between the gas and solid phases is described phenomenologically by a single volumetric exchange coefficient K_{jk}, which corresponds to species exchange between the jth solid phase tank and kth gas phase tank. This coefficient lumps the physical effects of species transport between the gas film and solid particle, as well as the finite rates of adsorption and surface transport of species on the catalyst surface, into a single parameter.
- For the kinetics of Centi et al. [11], the loss of surface oxygen from the catalyst cannot be explicitly accounted for since the kinetics are based on overall fixed bed data. For this reason, the approach of Pugsley et al. [25] is used where parallel deactivation of the catalyst is assumed. The kinetic parameters of deactivation are listed in Table 1.
- For the kinetics of Mills et al. [21] (Table 2), it is assumed that the VPO catalyst enters the riser in a fully oxidized state, and that any gas phase oxygen, if present in the riser, does not re-oxidize any catalyst. Thus, the concentration of gas phase oxygen in the partial oxidation of n-butane on the catalyst surface has no effect.
- Homogenous combustion of the hydrocarbon species in the gas phase is also considered with rate constants and kinetics obtained from Flagan and Seinfeld [26].

2.2. Model equations

The model formulation is based upon the representation given in Fig. 1. Based on the above set of assumptions, the following governing equations of the model can be developed, where $j \in [1, M]$, $k \in [1, N]$ and $i \in [1, NS]$.

Mass balance for species i in the jth solid phase tank:

$$\frac{W_{s,j}}{\rho_b}\frac{dC_{i,j}}{dt} = \frac{Q_s}{\rho_b}(C_{i,j-1} - C_{i,j}) + \sum_{p=1}^{N} K_{jp}(C_{i,p} - C_{i,j}) - \bar{R}_{s,i} W_{s,j} \quad (4)$$

Mass balance for species i in the kth gas phase tank:

$$V_{g,k}\frac{dC_{i,k}}{dt} = Q_g(C_{i,k-1} - C_{i,k}) - \sum_{q=1}^{M} K_{qk}(C_{i,k} - C_{i,q}) - \bar{R}_{h,i} V_{g,k} \quad (5)$$

The initial condition is

$$\text{at } t = 0: \quad C_j = C_k \quad \forall j, k \quad (6)$$

The reaction rate terms that appear above represent sink terms for reactants and source terms with the appropriate stoichiometric coefficient for the reaction products. The reaction rate in Eq. (4) refers to heterogeneous reaction on the catalyst surface, while that

Table 3
Dimensionless groups

Dimensionless group	Expression	Physical interpretation
Effective Stanton number (solid phase)[a]	$St_s = \frac{K\rho_b}{Q_s}$	$\frac{\text{Characteristic solids transport time}}{\text{Characteristic interphase mass transport time}}$
Effective Stanton number (gas phase)[a]	$St_g = \frac{K}{Q_g}$	$\frac{\text{Characteristic gas transport time}}{\text{Characteristic interphase mass transport time}}$
Peclet number (lattice oxygen diffusion)	$Pe_{LO} = \frac{\delta^2 Q_s}{MW_s D_{LO}}$	$\frac{\text{Characteristic lattice oxygen diffusion time}}{\text{Characteristic solids transport time}}$
Damkohler number (heterogeneous reactions)	$Da_s = \frac{W_s \rho_b \bar{R}_{s,i}}{c_{B_0} Q_s}$	$\frac{\text{Characteristic solids transport time}}{\text{Characteristic heterogeneous reaction time}}$
Damkohler number (homogeneous reactions)	$Da_g = \frac{MW_s \bar{R}_{h,i}}{N c_{B_0} Q_s}$	$\frac{\text{Characteristic solids transport time}}{\text{Characteristic homogeneous reaction time}}$

[a] These two numbers are not independent.

in Eq. (5) refers to homogeneous reaction in the gas phase. Definitions for the remaining terms and units are given in the Nomenclature.

It should be noted that when the redox kinetic model for VPO is used [21], no explicit source term for replenishment of the surface lattice oxygen by sub-surface lattice oxygen is necessary. This is already included in the transient particle-scale model, which is summarized in Mills et al. [21]. The model needs to be solved at each time-step to yield the local surface lattice oxygen concentration, which is used in the overall reaction rate that appears in the reactor scale model presented in Eqs. (4)–(6). The particle-scale model was solved using the public domain PDE collocation solver PDECOL [27], and was coupled to the reactor model and subsequently solved using a fourth-order Runge–Kutta method.

Eqs. (4)–(6) can be made dimensionless by scaling the species concentrations using both the initial gas phase *n*-butane concentration c_{B_0}, and the mean residence time of solids, τ_s. This leads to five dimensionless groups in the model equations, which are tabulated in Table 3. Since the kinetics and the lattice oxygen diffusion characteristics of the catalyst are pre-determined, the key dimensionless group of interest is the effective solids Stanton number St_s, which represents the ratio of the mean residence time of the solids to the characteristic mass transport time. Inspection of dimensional equations (4)–(6) shows that in their primitive form, the flow pattern parameters (N, M) are not independent of the cross-mixing parameter K, which represents the total mass transport rate in the reactor. However, St_s is innocent of these terms and emerges as an independent model parameter. Thus, even though numerical simulation of the model is expedited by using the original dimensional forms (4)–(6), the dimensionless forms are used for interpretation of the model predictions.

3. Results and discussion

3.1. Gas–solid flow simulation

A riser having the same dimensions given by Pugsley et al. [25] with a superficial gas velocity of $5\,m\,s^{-1}$ was simulated in two-dimensional axisymmetric coordinates using the FLUENT® CFD package. Here, both the solid and gas were considered to be interpenetrating fluids and their distributions at any particular location at a given instant of time in the reactor are described by their respective volume fractions. Based on this assumed picture of the reactor, which is macroscopic when compared to the particle size or eddies in gas phase, the two-fluid model equations were solved for the velocity distribution and volume fraction of each phase. The forces that are explicitly accounted for in the simulation are: (i) drag (momentum transfer) between the solid and gas phases; (ii) particle–particle interactions in the solid phase (following the work of Sinclair and Jackson [28]); (iii) turbulence in the gas phase. The interactions between solid particles are included by solving an extra equation for the pseudo-thermal temperature. The collisions between

Table 4
Parameters used in the 2D axisymmetric simulation of gas–solids riser

Column height	20 m
Column diameter	1.5 m
Grid	400 (axial)×20 (radial)
Cell size	0.05 m (axial)×0.0375 m (radial) (uniform grid)
Time step	0.01 s
Iterations per time step for convergence	around 25
Particle size	80 μm
Superficial gas velocity	5 m s^{-1}
Drag formulation	Wen and Yu [38]
Particle interaction model	Sinclair and Jackson [28]
Gas phase turbulence model	Two-phase k–ε model [40]

the solid particles and riser wall are incorporated in a boundary condition [32]. The other assumptions made in the simulation and the model equation are discussed elsewhere [28–32]. The model parameters used in the CFD simulation are summarized in Table 4.

A summary of the key parameters that were evaluated from the CFD simulation is given in Table 5. Typical results from the CFD simulation are presented in Fig. 2. The time-averaged velocity profile given in Fig. 2a shows that the solids flow up in the center of the column and flow downward in the periphery, which is typically observed in cold-flow units [24]. Fig. 2b shows that the solids concentration profile is quite flat at the central core of the column and rises steeply in the annular region at the wall. Thus, a significant fraction of the solid inventory (26.8% by weight) is actually downflowing in the time-averaged sense, which contributes to significant backmixing of the solid phase.

Once the velocity and holdup profiles in the simulation were fully developed, a second simulation was performed by tagging both the solid and gas phases by inert scalars that were uniformly distributed at the inlet. The flow of these inert scalar tracers, which are also non-volatile and hence remain confined to the given phase, was evaluated as a function of time and the concentration of these species was monitored and flow-averaged at the exit of the riser, to yield the mixing cup tracer concentrations. By normalizing these concentrations, the residence time distribution (RTD) curves of each phase were obtained. The simulated responses are shown in Fig. 3. The mean residence times of the phases, as well as the variance of the RTD curves, were calculated and are listed in Table 5. This shows that for the particular process variables used here, the gas and solids have mean residence times of 41 and 53 s, respectively. These simulation results provide an estimate of the gas and solids mixing that can otherwise only be obtained by conducting experimental tracer-response experiments.

Table 5
Parameters evaluated from 2D axisymmetric simulation of gas–solids riser

Mean solids holdup	0.086
Mean solids flux	∼130 kg s^{-1}
Total solids inventory	∼5200 kg
Mean residence time of solids	53 s
Mean residence time of gas	41 s
Dimensionless variance (solids)	0.434
Dimensionless variance (gas)	0.237
Equivalent number of tanks (solids)	∼2
Equivalent number of tanks (gas)	∼4

3.2. Reactor simulation

3.2.1. Effect of gas and solids mixing

The phenomenological model described in Section 2.2 was evaluated using the operating variable parameters listed in Table 3, the mixing parameters obtained from CFD flow simulation in Table 5, and the variable reactor model parameters given in Table 6. Using the same set of flow conditions and mixing parameters, the model predictions were evaluated using both the kinetics of Centi et al. [11] and Mills et al. [21] to assess the presence and absence of gas phase oxygen on reactor performance.

Using the fixed mean residence times of gas and solid phase that were evaluated from the flow simulation (see Table 5), the effect of mixing in either of the

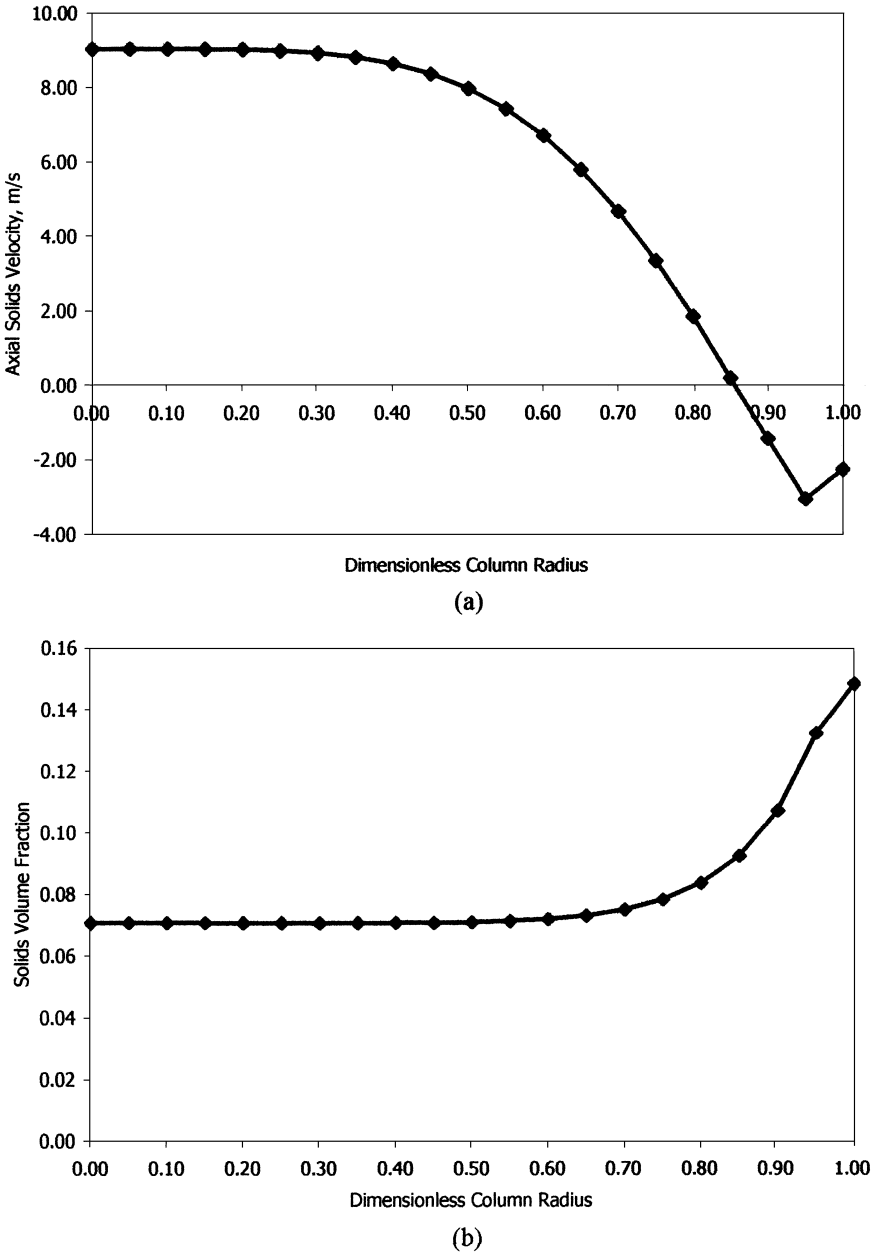

Fig. 2. CFD simulation of time-averaged solids flow pattern in the riser. (a) Axial solids velocity profile; (b) solids volume fraction distribution.

solid and gases phases on performance was investigated. The results are shown in Table 7 for the kinetics of Centi et al. [11] and in Table 8 for the kinetics of Mills et al. [21]. It is clear from the conversion versus yield data in these tables that the preferred scheme of contacting for optimizing reactor performance is to approach plug flow for both the solid and gas phases, and that both conversion and yield approaches an asymp-

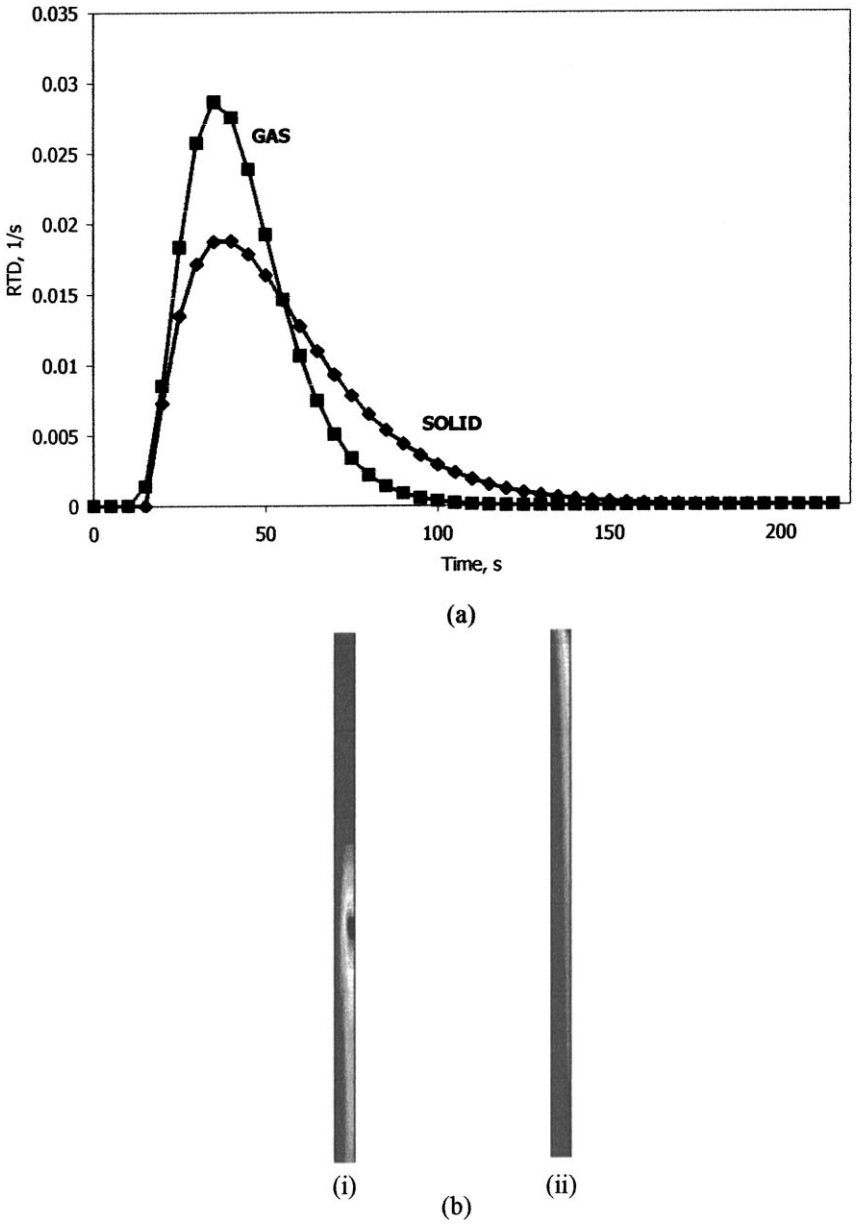

Fig. 3. (a) Solids and gas phase RTD from CFD simulation. (b) A snapshot of evolution of the solid phase tracer (i) just after injection; (ii) after tracer is flowing out at the exit of the riser (red: high concentration; blue: low concentration).

tote with an increasing number of compartments in either phase.

In general, the kinetic scheme of Mills et al. [21] seems to predict a much lower yield of MAN, even though the overall conversion of *n*-butane is high. While such a trend is a function of many variables, the parallel reaction scheme reported by Mills et al. [21] (Table 2) suggests that the reactions for the complete oxidation of *n*-butane to CO and CO_2 are preferentially favored. This is the case since these reactions have higher orders with respect to lattice oxygen and this effect becomes more pronounced as plug flow is

Table 6
Other (floating) parameters used in reactor simulation[a]

Number of solids compartments	2
Number of gas compartments	4
Gas phase *n*-butane concentration in feed	1.865 mol m^{-3} (10% at 380°C)
Gas phase O_2 concentration in feed	10 mol m^{-3}
Exchange coefficient	10 m^3 s^{-1}
Catalyst deactivation	50% at exit[b]

[a] Sensitivity of the models to each of these parameters was studied. In any such analysis, values of the other parameters were fixed at the values presented in this table.
[b] Used only with kinetics of Centi et al. [11].

approached by an increasing number of mixing cells. Thus, while approaching plug flow patterns for both the gas and solid phases does result in better utilization of the catalyst, this benefit is partially offset by an increased yield of combustion products through the undesired parallel reactions. This is an issue of real industrial significance, since it shows that lattice oxygen indeed affects both the selective and non-selective products formed in butane oxidation [18,21]. It also illustrates that an optimum gas–solid contacting time exists for a given flow pattern of the gas and solid phases to achieve a maximum yield of MAN.

The reaction kinetics of Centi et al. [11] predicts a much higher yield of MAN when compared to those of Mills et al. [21]. The yield increases steadily as the flow pattern of both the solids and gas phases approach plug flow. More plug flow behavior promotes more of the desirable reaction and suppresses the undesirable oxidation of MAN. However, the loss of activity of the catalyst is only arbitrarily accounted for (50% deactivation at the exit in this case). Hence, a design that is based on such an assumption is likely to be in error for this reason.

Table 7
Effect of mixing pattern on *n*-butane conversion and MAN yield (kinetics of Centi et al. [11]) (K=10.0 m^3 s^{-1})

Number of solid compartments	Number of gas compartments[a]	Conversion of *n*-butane	Yield of MAN
1	1 (1)	73.3	19.3
	2 (2)	78.1	24.2
	3 (3)	78.6	24.7
	4 (4)	78.6	24.8
	5 (5)	78.6	24.8
	6 (6)	78.6	24.8
2	2 (1)	80.2	27.9
	4 (2)	82.7	28.1
	6 (3)	82.9	28.4
	8 (4)	83.0	28.5
3	3 (1)	85.9	29.8
	6 (2)	88.0	31.6
	9 (3)	88.6	32.0

[a] Numbers in parentheses show the number of gas phase compartments exchanging mass with each solid phase compartment.

Table 8
Effect of mixing pattern on *n*-butane conversion and MAN yield (kinetics of Mills et al. [21]) (K=1.0 m^3 s^{-1})

Number of solid compartments	Number of gas compartments[a]	Conversion of *n*-butane	Yield of MAN
1	1 (1)	40.5	4.8
	2 (2)	61.7	7.8
	3 (3)	73.4	9.5
	4 (4)	79.9	10.4
	5 (5)	83.7	10.9
	6 (6)	85.7	11.3
2	2 (1)	62.0	7.8
	4 (2)	81.6	10.6
	6 (3)	89.0	11.7
	8 (4)	98.4	12.9
3	3 (1)	74.4	9.6
	6 (2)	89.6	11.8
	9 (3)	98.6	13.3

[a] Numbers in parentheses show the number of gas phase compartments exchanging mass with each solid phase compartment.

3.2.2. Effect of exchange between phases

In addition to accounting for the impact of gas and solid backmixing through variation of the number of compartments, the other key parameter in the present model is the exchange coefficient K. Conceptually, this represents the transport of reactants and products between the bulk gas phase and the particle surface. The importance of the mass transport rate (incorporated in K) relative to the corresponding phase mean residence times is expressed as the dimensionless Stanton number for the gas and solid phases St_s and St_g, respectively. A value of St_s=0 represents the case where no exchange occurs and consequently no reaction, except for the homogeneous oxidation reactions in the gas phase. A very high value of St_s describes the situation where the species enters the reactor directly in the solid phase since the transport resistance

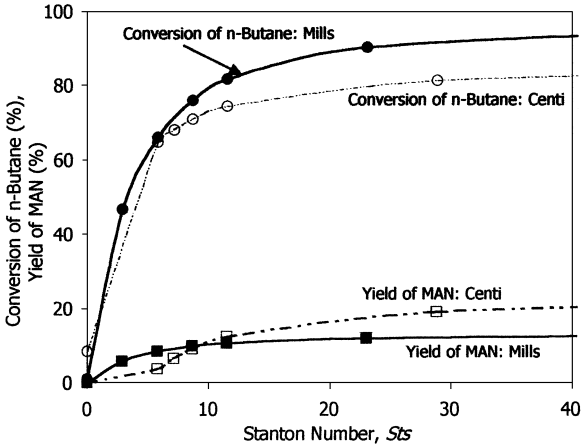

Fig. 4. Effect of variation of the Stanton number on overall performance of the reactor.

between the solid and gas phases is negligible and the kinetic resistance is controlling.

The effect of varying the exchange coefficient on the overall reactor performance is shown in Fig. 4 for both the kinetics of Centi et al. [11] and Mills et al. [21]. Stanton numbers of 25 or more are sufficiently high to produce nearly constant conversions and yields from both kinetic models. It is also apparent that the Stanton number has a slightly more pronounced effect when the Centi et al. [11] kinetics are used, since this kinetic model requires transport of both *n*-butane and MAN to the solid phase. Hence, the reactor performance becomes independent of mass transport effects at higher values of the Stanton number (Fig. 4) when compared to the model predictions based on the Mills et al. [21] kinetics. For this latter model, only transport of *n*-butane is required since the oxygen being supplied by the catalyst sub-surface.

3.2.3. Reactor efficiency

It is instructive to invoke the concept of reactor efficiency [33]. This parameter is defined as the ratio of the actual overall rate of formation of MAN in the riser reactor to the rate that would exist if all the catalyst were exposed to the gas phase reactants at feed conditions. Such a measure helps to quantify the influence of both the overall flow pattern and interphase contacting on deviation of the reactor performance from ideality. The results of this analysis are compared in Fig. 5 for the kinetics of Centi et al. [11] and Mills et al. [21], respectively. The results in Fig. 5 are presented using the gas–solids exchange coefficient as a parameter with three alternative flow patterns for the gas and solid phases.

The influence of the flow pattern, which is created by changing the number of mixing compartments in each phase, is more pronounced when the kinetics of Mills et al. [21] are used. For a given flow pattern, increasing the value of exchange coefficient initially results in an increase in the reactor efficiency, but further increases have no effect since the kinetics are apparently controlling the local rate.

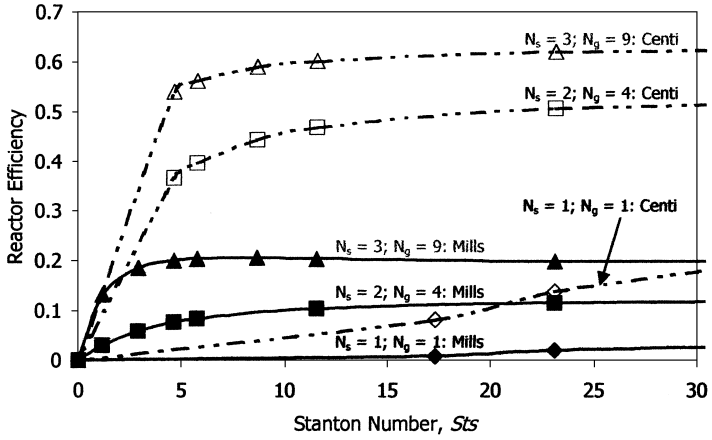

Fig. 5. Reactor efficiency as a function of backmixing and Stanton number.

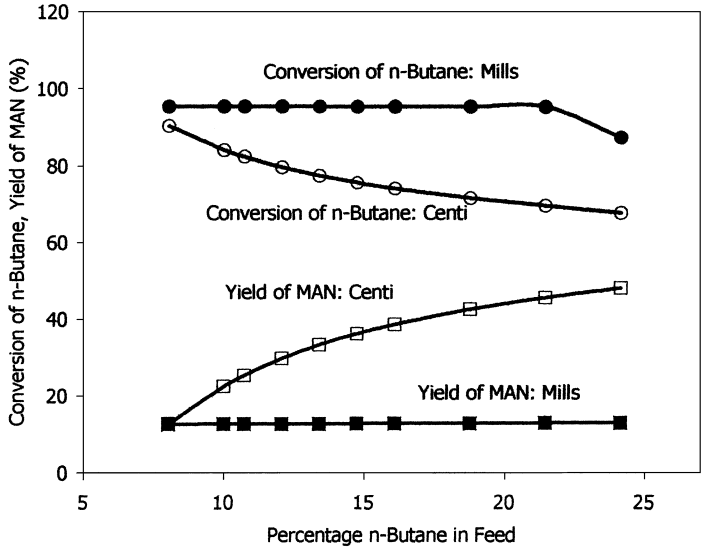

Fig. 6. Effect of variation of the feed *n*-butane concentration on overall performance of the reactor. (a) Kinetics of Centi et al. [11]; (b) kinetics of Mills et al. [21].

3.2.4. Effect of butane feed concentration

Overall reactor performance should be affected by the molar ratio of *n*-butane and oxygen ratio in the feed gas. Fig. 6 compares the effect of increasing the concentration of *n*-butane on both the conversion of *n*-butane and the MAN yield using a fixed oxygen concentration of 10 mol m^{-3}. Model predictions with the kinetic model of Centi et al. [11] show that increasing the percentage of *n*-butane in the feed gas leads to an increase in the yield of MAN. The overall conversion of *n*-butane decreases with an increase in the butane feed concentration since the loss of *n*-butane to the undesired side reactions is also less. With the kinetics of Mills et al. [21], the model indicates that the *n*-butane

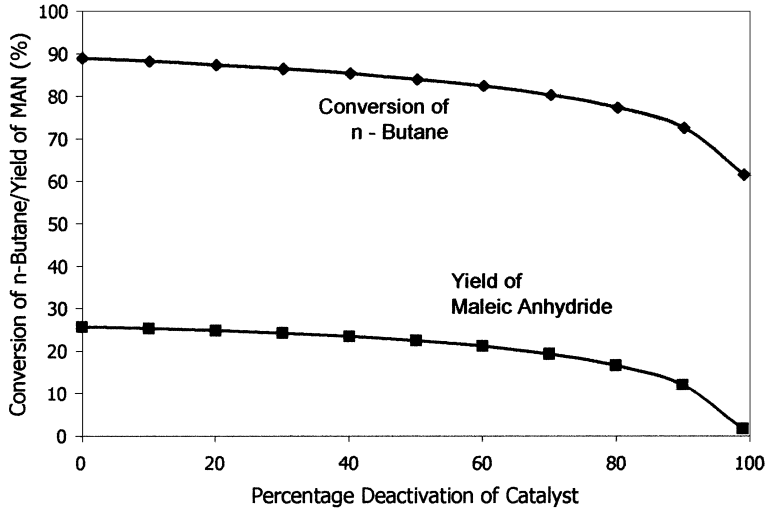

Fig. 7. Effect of catalyst deactivation on reactor performance (with the kinetics of Centi et al. [11]).

conversion and MAN yield are insensitive to the percentage of *n*-butane in the feed. The latter result can be explained by referring to Table 2, where it can be seen that the proposed parallel reaction scheme involves reactions that are all first order with respect to *n*-butane. Hence, both the point selectivity and the overall yield are insensitive to the *n*-butane concentration.

3.2.5. Effect of catalyst deactivation

The effect of the extent of catalyst deactivation on the reactor performance was also briefly investigated. Following the work of Pugsley et al. [25], the catalyst was assumed to undergo parallel deactivation. Hence, the extent of catalyst deactivation is a parameter that also determines the reactor performance. Fig. 7 shows that both the overall *n*-butane conversion and MAN yield will decrease if the catalyst is allowed to deactivate. Other various mechanisms of catalyst deactivation can be envisioned, but this illustrates what degree of reduction in performance can be expected for a given percentage of catalyst deactivation.

4. Summary and conclusions

To provide a reasonably accurate basis for assessment of the gas and solids flow patterns, the fundamental fluid dynamic equations that describe multiphase flow in a gas–solid riser reactor of known geometry were solved using a commercially available CFD code. The appropriate gas–solid momentum transport interactions and constitutive relations were described by invoking a treatment of the granular solid phase based on kinetic theory. The detailed gas and solid velocities and holdup profiles obtained from the simulation were used to evaluate the exit-age probability density distributions of both the gas and solid phases.

A phenomenological cell-type model that accounted for gas–solid interactions was developed for the riser reactor as part of an effort to mimic the macroscopic gas and solid flow patterns that were extracted from the CFD simulation. The reactor performance was compared using two different reaction kinetic models from the literature for butane oxidation to MAN and carbon oxides over VPO catalysts. The first kinetic model, which is based upon the work of Centi et al. [11], did not explicitly account for solid-state diffusion of lattice oxygen and was mainly used to benchmark the findings of the proposed riser reactor hydrodynamic model. The second kinetic model kinetic scheme, which was based upon the recent work of Mills et al. [21], explicitly incorporated the role of lattice oxygen diffusion in the catalyst bulk. It described the reduction of VPO by *n*-butane in the absence of gas phase oxygen from which both MAN and carbon oxides were formed through a parallel reaction network.

The results of various riser model simulations show that the kinetic model of Centi et al. [11] predicts yields of MAN that are notably greater than those predicted from the kinetic model of Mills et al. [21]. This mainly occurs since each kinetic model is based upon a notably different range of experimental conditions, which points to the need to use caution when using literature kinetics for preliminary reactor design purposes. For the riser operation mode that is used here, the kinetic model of Mills et al. [21] is more applicable since it was measured under conditions that mimic the cyclic exposure of the VPO catalyst to *n*-butane and oxygen.

Acknowledgements

One of the authors (SR) would like to acknowledge Ms. Garima Bhatia for the help extended with implementation of the PDECOL routines in the particle-scale model. Both the authors (SR and MPD) would like to thank industrial sponsors of CREL for their financial support.

References

[1] T.R. Felthouse, J.C. Burnett, S.F. Mitchell, M.J. Mummey, Maleic anhydride, maleic acid and fumaric acid, in: Kirk-Othmer Encyclopedia of Chemical Technology, Vol. 15, 4th Edition, Wiley, New York, 1995, p. 893.
[2] R.K. Sharma, D.L. Creswell, Paper presented at the AIChE Annual Meeting, San Francisco, CA, 1984.
[3] R.M. Contractor, A.W. Sleight, Maleic anhydride from C-4 feedstocks using fluidized bed reactors, Catal. Today 1 (5) (1987) 587.
[4] W. Stadig, Three inventions combine to yield new route to THF, Chem. Process. (1992) 18.
[5] J. Haggin, Innovations in catalysis create environmentally friendly THF process, Chem. Eng. News (1995) 20.
[6] R.M. Contractor, DuPont's CFB technology for maleic anhydride from conception to commercialization, in:

Proceedings of the Sixth International Conference on Circulating Fluidized Beds, 1999.
[7] G. Centi, F. Trifiro, J.R. Ebner, V.M. Franchetti, Mechanistic aspects of maleic anhydride synthesis from C_4 hydrocarbons over phosphorus vanadium oxide, Chem. Rev. 88 (1988) 55.
[8] A. Escardino, Catalytic oxidation of butane to maleic anhydride. I. Mechanism of the reaction, An. Quim. 69 (3) (1973) 385.
[9] J.S. Buchanan, S. Sundaresan, Kinetics and redox properties of vanadium phosphate catalysts for butane oxidation, Appl. Catal. 26 (1986) 211.
[10] J.J. Lerou, J.F. Weiher, Paper Presented at the Pittsburgh/Cleveland Catalysis Society Meeting, USA, 1986.
[11] G. Centi, G. Fornasari, F. Trifiro, *n*-Butane oxidation to maleic anhydride on vanadium phosphorus oxides: kinetic analysis with tubular flow stacked pellet reactor, Ind. Eng. Chem., Proc. Res. Dev. 24 (1985) 32.
[12] P. Schneider, G. Emig, H. Hofmann, Kinetic investigation and reactor simulation for the catalytic gas-phase oxidation of *n*-butane to maleic anhydride, Ind. Eng. Chem. Res. 22 (1987) 2236.
[13] B.K. Hodnett, Vanadium-phosphorus oxide catalysts for the selective oxidation of C_4 hydrocarbons to maleic anhydride, Catal. Rev.-Sci. Eng. 27 (3) (1985) 373–424.
[14] R.K. Sharma, D.L. Creswell, E.J. Newson, Kinetics and fixed-bed reactor modeling of butane oxidation to maleic anhydride, AIChE J. 37 (1) (1991) 39.
[15] S.K. Bej, M.S. Rao, Selective oxidation of *n*-butane to maleic anhydride. 1. Optimization studies, Ind. Eng. Chem. Res. 30 (8) (1991) 1819.
[16] S.K. Bej, M.S. Rao, Selective oxidation of *n*-butane to maleic anhydride. 2. Identification of rate expression for the reaction, Ind. Eng. Chem. Res. 30 (8) (1991) 1824.
[17] S.K. Bej, M.S. Rao, Selective oxidation of *n*-butane to maleic anhydride. 3. Modeling studies, Ind. Eng. Chem. Res. 30 (8) (1991) 1829.
[18] S.K. Bej, M.S. Rao, Selective oxidation of *n*-butane to maleic anhydride. 4. Recycle reactor studies, Ind. Eng. Chem. Res. 31 (9) (1992) 2075.
[19] D. Dowell, J.T. Gleaves, Y. Schuurman, The nature of active/selective phase in VPO catalysts and the kinetics of *n*-butane oxidation, in: Proceedings of the Third World Congress on Oxidation Catalysis, 1997, Stud. Surf. Sci. Catal. 110 (1997) 199.
[20] Y. Schuurman, J.T. Gleaves, A comparison of steady-state and unsteady state reaction kinetics of *n*-butane oxidation using the TAP-2 reactor system, Catal. Today 33 (1–3) (1997) 25.
[21] P.L. Mills, H.T. Randall, J.S. McCracken, Redox kinetics of $VOPO_4$ with butane and oxygen using the TAP reactor system, in: Proceedings of the ISCRE 15, Chem. Eng. Sci. 54 (13–14) (1999) 3709.
[22] J.S. McCracken, P.L. Mills, TAP reactor system hardware improvements at DuPont, Paper Presented at the Second International Conference on Unsteady State Processes in Catalysis, Section on Studies of Catalyst Surface Dynamics, St. Louis, MO, 1995.
[23] L. S. Fan, C. Zhu, Principles of Gas–Solid Flows, Cambridge University Press, Cambridge, 1998.
[24] M.J. Rhodes, P. Lausman, F. Villain, D. Geldart, Measurement of radial and axial solids flux variations in the riser of a circulating fluidized bed, in: P. Basu, J.F. Largo (Eds.), Circulating Fluidized Bed Technology, Pergamon Press, Toronto, 1988, pp. 155–164.
[25] T.S. Pugsley, G.S. Patience, F. Berruti, J. Chaouki, Modeling the catalytic oxidation of *n*-butane to maleic anhydride in a circulating fluidized bed reactor, Ind. Eng. Chem. Res. 31 (1992) 2652.
[26] R.C. Flagan, J.H. Seinfeld, Fundamentals of Air Pollution Engineering, Prentice-Hall, Englewood Cliffs, NJ, 1988.
[27] R.F. Sincovec, N.K. Madsen, Software for non-linear partial differential equations, Assoc. Comput. Machinary-TOMS 1 (3) (1975) 232.
[28] J.L. Sinclair, R. Jackson, The effect of particle–particle interaction on the flow of gas particles in a vertical pipe, AIChE J. 35 (1989) 1473.
[29] Y.P. Tsuo, D. Gidaspow, Computation of flow pattern in circulating fluidized beds, AIChE J. 36 (1990) 885.
[30] C.M. Hrenya, J.L. Sinclair, Effects of particle phase turbulence in gas–solid flows, AIChE J. 43 (4) (1997) 853.
[31] C.K.K. Lun, S.B. Savage, D.J. Jeffrey, N. Cherpuniy, Kinetic theories for granular flow: inelastic particles in Couette flow and slightly inelastic particles in a general flow field, J. Fluid Mech. 140 (1984) 223.
[32] P.C. Johnson, R. Jackson, Frictional–collisional constitutive relations for granular materials, with applications to plane shearing, J. Fluid Mech. 176 (1987) 67.
[33] P.A. Ramachandran, R.V. Chaudhari, Three-Phase Catalytic Reactors, Gordon and Breach, London, 1983.